Dalton Transactions

PAPER

Preparation and confinement effect of a heterogeneous 9-amino-9-deoxy-*epi*-cinchonidine organocatalyst for asymmetric aldol addition in aqueous medium†

Wei Wang, Xuebing Ma,* Jingwei Wan, Jun Cao and Qian Tang

A series of novel porous zirconium phosphonate-supported 9-amino-9-deoxy-*epi*-cinchonidines of general formulae $Zr(OH)_{4-2x}(O_3PR)_x \cdot nH_2O$ and $Zr(HPO_4)_{2-x}(O_3PR)_x \cdot nH_2O$ with the different arm chain lengths ($n = 2$–6) and mean diameters of approximately 20–40 nm have been prepared as heterogeneous organocatalysts. The different microtextures of zirconium phosphonates were also obtained by using template guest molecules, such as Et_3N, NaH_2PO_4 and sodium dodecyl benzene sulfonate. In the heterogeneous asymmetric aldol addition of *p*-nitrobenzaldehyde to cyclohexanone, excellent catalytic properties were achieved, especially in an aqueous medium. After completing the reaction, those zirconium phosphonate-supported 9-amino-9-deoxy-*epi*-cinchonidine organocatalysts could be readily recovered in quantitative yield by centrifugation or filtration, and reused for five consecutive runs without significant loss in catalytic performance. In particular, due to the steric confinement effect of the inorganic backbone, the single different configuration among possible four stereo-isomers in aldol adducts were favorably obtained, respectively depending on the interaction between the *o*-, *m*- or *p*-position of nitrobenzaldehyde and the backbone, which was never observed in homogeneous aldol addition.

Introduction

The direct asymmetric aldol reaction is one of the most important C–C bond-forming reactions in synthetic chemistry and is of much importance in pharmaceutical, agrochemical, and fine chemical industries. The design and preparation of highly selective asymmetric organocatalysts for aldol reaction has attracted much attention and excellent results have been achieved.[1] However, due to economic consideration of different organocatalysts, the development, recycling and reuse of these organocatalysts is currently a highly sought after goal and urgently desired for our chemists. Several approaches, including fluorous proline derivatives,[2] solid phase-supported catalysts,[3] ionic liquids,[4] PEG[5] or aqueous media as reaction solvent, have been used to achieve organocatalyst recovery. Among these strategies, water as solvent is an environmentally friendly, safe reaction medium from a practical perspective, which avoids the problem of pollution that is inherent with organic solvent. In fact, some proline amide derivatives or small peptides have proved useful for catalyzing aldol reactions with high enantioselectivity in aqueous media.[6]

A number of cinchona derivatives have been versatile organocatalysts in many asymmetric organic transformations owing to their excellent performances.[7] For example, 9-amino-9-deoxy-*epi*-cinchonine, one of the most famous cinchona derivatives, has been employed as an efficient organocatalyst with excellent stereoselectivity and activity in asymmetric aldol addition,[8] Diels–Alder reaction,[9] Friedel–Crafts reaction,[10] Henry reaction,[11] Mannich reaction,[12] Michael addition,[13] hydrogenation,[14] epoxidation,[15] 1, 3-dipolar cycloaddition,[16] decarboxylation,[17] and methanolytic desymmetrization.[18] However, the potential application of those organocatalysts in chemical industry is rather limited owing to their high cost of chemical transformation. Unfortunately, although the well-known 9-amino-9-deoxy-*epi*-cinchonine organocatalyst possessed excellent performance in many organic asymmetric transformations, its recycling and reusability in the catalytic process are seldom reported. Just in 2008, it was reported that 9-thiourea cinchona alkaloid supported on mesoporous silica was used as a highly enantioselective, recyclable heterogeneous organocatalyst in the asymmetric Friedel–Crafts reaction of imines with indoles.[19]

In the last thirty years, an emerging class of insoluble phosphonates and inorganic–organic phosphonates of tetravalent metals (mainly Zr^{IV}) with layered or pillared structure have attracted the attention of researchers because of their interesting

College of Chemistry and Chemical Engineering, Southwest University, Chongqing, 400715, P.R. China. E-mail: zcj123@swu.edu.cn; Fax: (+86)23-68253237; Tel: (+86)23-68253237
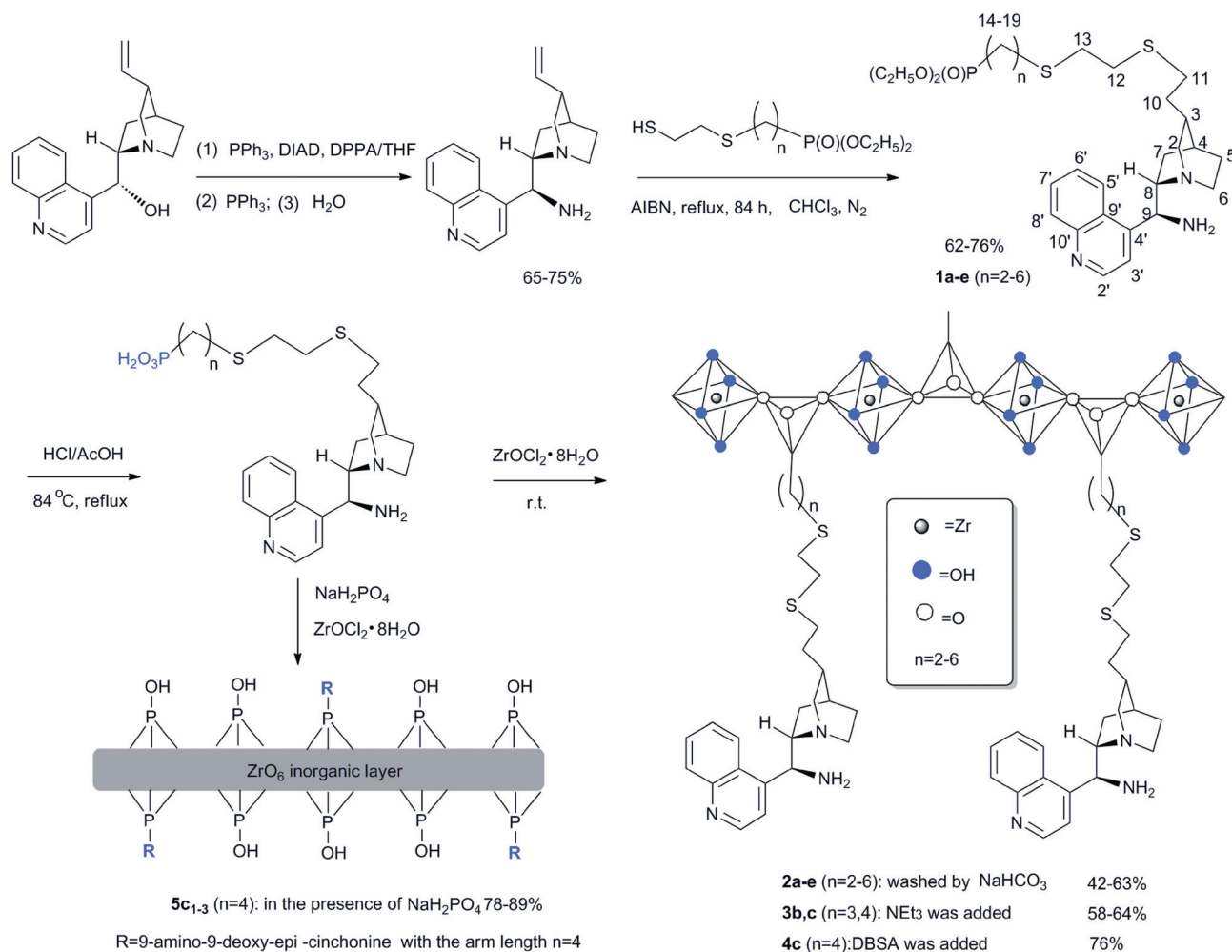
Scheme 1 The synthetic route to supported 9-amino-9-deoxy-*epi*-cinchonine organocatalysts.

physical–chemical properties and high versatility,[20] especially in the field of catalysis.[21] The layered and porous inorganic backbone of zirconium phosphate may be considered as a hook onto which organic groups with different functionality may be attached, allowing for the control of both reactivity and selectivity in organic catalytic processes.[22] Such a molecular building block approach towards heterogeneous asymmetric catalysis will represent a major advance in chirotechnology owing to both its tunability as well as reusability.

Recently, we have been involved in the development of novel chiral organocatalysts to be used in benign reaction media, such as water, for the definition of chemically and environmentally efficient organic processes. In this paper, we developed a novel type of heterogeneous, porous and recycled zirconium phosphonate-supported 9-amino-9-deoxy-*epi*-cinchonine organocatalysts with the different arm lengths (*n* = 2–6) (Scheme 1). In the asymmetric direct aldol addition of *p*-nitrobenzaldehyde to cyclohexanone, the high catalytic properties (98% yield, *anti/syn* = 83 : 17 and 96%ee *anti*) and reusability were achieved in water as sole reaction medium. Especially, due to the steric confinement effect of the inorganic backbone of zirconium phosphonate, one single configuration among the possible four stereo-isomers in aldol adducts was favorably obtained, depending on the *o*-, *m*-

or *p*-position of nitrobenzaldehyde, which was never observed in homogeneous aldol addition.

Experimental

Materials and sample characterization

All chemicals were purchased and used without any further purification. The starting materials 9-amino-9-deoxy-*epi*-cinchonine and $HS(CH_2)_2S(CH_2)_nP(O)(OC_2H_5)_2$ (*n* = 2–6) were synthesized according to the reference and ascertained by ^{1}H and ^{13}C NMR.[22d]

TLC, where applicable, was performed on pre-coated aluminum-backed plates and spots were made visible by quenching ultraviolet fluorescence (λ = 254 nm). Fourier transform infrared spectra were recorded on a Perkin-Elmer Model GX Spectrometer using a KBr pellet method with polystyrene as a standard. Thermogravimetric analysis (TGA) was performed on a SBTQ 600 Thermal Analyzer (USA) with a heating rate of 20 °C min^{-1} over a temperature range of 40–800 °C under flowing compressed N_2 (100 mL min^{-1}). ^{1}H, ^{13}C and ^{31}P NMR were performed on a Bruker AV-300 NMR instrument at ambient temperature at 300, 75, and 121 MHz, respectively. All chemical

shifts were reported downfield in ppm relative to the hydrogen, carbon, and phosphorus resonance of TMS, chloroform-d_1, and H_3PO_4 (85%), respectively. The interlayer spacings of samples were obtained on a DX-1000 automated X-ray power diffractometer (XRD), using Cu $K\alpha$ radiation and internal silicon powder as a standard with all samples. The patterns were measured between 2.00° and 20.00° (2θ) with a step size of 1° min^{-1} and X-ray tube settings of 40 kV and 2.5 mA. C, H, and N elemental analysis was obtained from an EATM 1112 automatic elemental analyzer instrument (Thermo, USA). The morphologies of the as-synthesized samples were determined by a Hitachi model H-800 transmission electron microscope (TEM) and a Multimode SPM atomic force microscopy (AFM). N_2 adsorption–desorption analysis was carried out at 77 K on an Autosorb-1 apparatus (Quantachrome). The specific surface areas and pore diameters were calculated by the BET method and BJH model, respectively. The *anti/syn* ratio of aldol product was determined by ^1H NMR of crude product and the enantiomeric excess (%ee) was determined on HPLC with a Chiral OD or AD column (*n*-hexane/2-propanol = 95/5) under 20 °C, 254 nm and 0.5 mL min^{-1} conditions.

General procedure for phosphonates 1a–e

To a flask (100 mL) was charged with 9-amino-9-deoxy-*epi*-cinchonine (3.1 g, 10.6 mmol), $HS(CH_2)_2S(CH_2)_nP(O)$-(O $C_2H_5)_2$ (*n* = 2–6) (42.2 mmol) and AIBN (0.43 g, 2.6 mmol), flushed three times with Ar atmosphere and sealed. Then $CHCl_3$ (60 mL) were added by a syringe and the reaction mixture was refluxed for 72 h at 80 °C with the tracking of TLC. During the reaction, AIBN (0.43 g, 2.6 mmol) was added once per 24 hours. The reaction residue was concentrated under reduced pressure, adjusted by 10% HCl solution to pH = 1 and extracted by ethyl acetate (70 mL × 4). In the aqueous phase concentrated ammonia was added to pH = 10 and extracted by CH_2Cl_2 (70 mL × 4). The combined organic phase was washed with saturated ammonium chloride (50 mL × 3) and brine (50 mL × 3), dried over anhydrous Na_2SO_4, and concentrated under reduced pressure. The crude products were purified by gradient silica gel column chromatography using $CHCl_3$/petroleum ether (v/v = 2/1) to remove the unreacted $HS(CH_2)_2S(CH_2)_nP(O)$-$(OC_2H_5)_2$ (*n* = 2–6) and then $CHCl_3$/methanol (v/v = 80/1 → 60/1 → 40/1 → 20/1) as the eluents to afford the brown viscous and oily **1a–e**.

Phosphonate 1a. (3.6 g, 62%), brown oily liquid. δ_H (300 MHz, CDCl$_3$, Me$_4$Si) 8.87 (1 H, d, ^3J = 6.0 Hz, H-2′), 8.34 (1 H, d, ^3J = 9.0 Hz, H-5′), 8.13 (1 H, d, ^3J = 9.0 Hz, H-8′), 7.68 (1 H, t, ^3J = 6.0 Hz, H-7′), 7.59 (1 H, t, ^3J = 6.0 Hz, H-6′), 7.55 (1 H, d, ^3J = 2.0 Hz, H-3′), 4.72 (1 H, d, ^3J = 9.0 Hz, H-9), 4.08 (4 H, m, –OCH$_2$), 3.22–3.30 (2 H, m, H-6α, H-2-*exo*), 3.09 (1 H, d, ^3J = 9.0 Hz, H-8), 2.70–2.79 (8 H, m, H-14, H-12, H-13, H-6β, H-2-*endo*), 2.44–2.56 (2 H, m, H-11), 1.95–2.07 (3 H, m, H-5α, H-15), 1.43–1.67 (6 H, m, H-3, H-4, H-5β, H-7β, H-10), 1.30 (6 H, t, ^3J = 6.0 Hz, CH$_3$), 0.76 (1 H, br s, H-7α). δ_C (75.0 MHz, CDCl$_3$) 150.1 (C-6′), 148.3 (C-4′), 140.2 (C-2′), 130.2 (C-10′), 128.9 (C-8′), 127.4 (C-9′), 126.4 (C-7′), 123.1 (C-3′), 119.4 (C-5′), 77.1 (C-8), 62.6 (C-2), 61.6 (OCH$_2$, d, $^2J_{C-P}$ = 6.8 Hz), 55.7 (C-9), 41.3 (C-6), 34.1 (C-13), 33.3 (C-3), 32.5

(C-15, $^1J_{C-P}$ = 42.8 Hz), 31.2 (C-12), 30.0 (C-11), 29.4 (C-5), 29.1 (C-7), 27.9 (C-14, d, $^2J_{C-P}$ = 18.0 Hz), 26.5 (C-4), 25.4 (C-10), 16.2 (CH$_3$, $^3J_{C-P}$ = 6.8 Hz). δ_P (121.0 MHz, CDCl$_3$) 29.4. Anal. calcd for C$_{27}$H$_{42}$N$_3$O$_3$PS$_2$: C, 58.78; H, 7.67; N, 7.62; Found: C, 58.85; H, 7.74; N, 9.57.

Phosphonate 1b. (4.0 g, 68%), brown oily liquid. δ_H (300 MHz, CDCl$_3$, Me$_4$Si) 8.84 (1 H, d, ^3J = 6.0 Hz, H-2′), 8.27 (1 H, d, ^3J = 9.0 Hz, H-5′), 8.07 (1 H, d, ^3J = 9.0 Hz, H-8′), 7.65 (1 H, t, ^3J = 6.0 Hz, H-7′), 7.54 (1 H, t, ^3J = 6.0 Hz, H-6′), 7.50 (1 H, d, ^3J = 2.0 Hz, H-3′), 4.64 (1 H, d, ^3J = 9.0 Hz, H-9), 4.00 (4 H, m, OCH$_2$), 3.05–3.27 (3 H, m, H-6α, H-2-*exo*, H-8), 2.38–2.60 (11 H, m, H-12, H-13, H-14, H-11, H-6β, H-2-*endo*, H-5α), 1.76–1.79 (4 H, m, H-16, H-15), 1.49–1.64 (6 H, m, H-3, H-4, H-5β, H-7β, H-10), 1.24 (6 H, t, ^3J = 6.0 Hz, CH$_3$), 0.71 (H-7α, dd, 1 H). δ_C (75.0 MHz, CDCl$_3$) 150.0 (C-6′), 148.1 (C-4′), 148.0 (C-2′), 130.2 (C-10′), 128.9 (C-8′), 127.4 (C-9′), 126.4 (C-7′), 123.1 (C-3′), 119.4 (C-5′), 77.0 (C-8), 62.6 (C-2), 61.6 (d, $^2J_{C-P}$ = 6.8 Hz, OCH$_2$), 55.7 (C-9), 41.3 (C-6), 34.1 (C-14), 32.2 (C-3), 32.0 (C-13), 31.3 (C-12), 31.2 (C-11), 29.9 (C-5), 29.1 (C-7), 27.2 (C-16, d, $^1J_{C-P}$ = 15.0 Hz), 25.4 (C-4), 23.2 (C-10), 22.1 (d, $^2J_{C-P}$ = 4.5 Hz, C-15), 16.1 (d, $^3J_{C-P}$ = 6.0 Hz, CH$_3$). δ_P (121.0 MHz, CDCl$_3$) 32.5. Anal. calcd for C$_{28}$H$_{44}$N$_3$O$_3$PS$_2$: C, 59.44; H, 7.84; N, 7.43; Found: C, 59.55; H, 7.87; N, 9.38.

Phosphonate 1c. (4.3 g, 70%), brown viscous and oily liquid. δ_H (300 MHz, CDCl$_3$, Me$_4$Si) 8.90 (1 H, dd, ^3J = 6 Hz, H-2′), 8.37 (1 H, d, ^3J = 9.0 Hz, H-5′), 8.14 (1 H, d, ^3J = 9.0 Hz, H-8′), 7.73 (1 H, t, ^3J = 6.0 Hz, H-7′), 7.54 (1 H, t, ^3J = 6.0 Hz, H-6′), 7.50 (1 H, d, ^3J = 2.0 Hz, H-3′), 4.77 (1 H, d, ^3J = 9.0 Hz, H-9), 4.09 (4 H, m, OCH$_2$), 3.24–3.32 (2 H, m, H-6α, H-2-*exo*), 3.07 (1 H, d, ^3J = 9.0 Hz, H-8), 2.38–2.68 (11 H, m, H-14, H-12, H-13, H-11, H-6β, H-2-*endo*, H-5α), 1.67–1.75 (6 H, m, H-15, H-16, H-17), 1.51–1.59 (6 H, H-3, H-4, H-5β, H-7β, H-10), 1.32 (6 H, t, ^3J = 6.0 Hz, CH$_3$), 0.76 (1 H, dd, H-7α). δ_C (75.0 MHz, CDCl$_3$) 150.2 (C-6′), 148.6 (C-4′), 148.3 (C-2′), 130.2 (C-10′), 128.9 (C-8′), 127.6 (C-9′), 126.4 (C-7′), 123.1 (C-3′), 119.4 (C-5′), 77.1(C-8), 61.7 (C-2), 61.3 (d, $^2J_{C-P}$ = 6.0 Hz, OCH$_2$), 57.4 (C-9), 40.7 (C-6), 34.4 (C-14, d, $^4J_{C-P}$ = 5.3 Hz), 33.0 (C-3), 32.4 (C-13), 32.0 (C-16, d, $^2J_{C-P}$ = 9.0 Hz), 31.4 (C-12), 30.2 (C-11), 30.1 (C-5), 28.4 (C-7), 26.0 (C-4), 25.4 (C-17, d, $^1J_{C-P}$ = 25.5 Hz), 24.1 (C-10), 21.4 (C-15, d, $^3J_{C-P}$ = 5.3 Hz), 16.2 (d, $^3J_{C-P}$ = 6.0 Hz, CH$_3$). δ_P (121.0 MHz, CDCl$_3$) 33.0. Anal. calcd for C$_{29}$H$_{46}$N$_3$O$_3$PS$_2$: C, 60.07; H, 8.00; N, 7.25; Found: C, 60.15; H, 8.08; N, 7.13.

Phosphonate 1d. (4.5 g, 72%), brown viscous and oily liquid. δ_H (300 MHz, CDCl$_3$, Me$_4$Si) 8.80 (1 H, dd, ^3J = 6.0 Hz, H-2′), 8.27 (1 H, d, ^3J = 9.0 Hz, H-5′), 8.04 (1 H, d, ^3J = 9.0 Hz, H-8′), 7.63 (1 H, t, ^3J = 6.0 Hz, H-7′), 7.51 (1 H, t, ^3J = 6.0 Hz, H-6′), 7.45 (1 H, d, ^3J = 2.0 Hz, H-3′), 4.61 (1 H, d, ^3J = 9.0 Hz, H-9), 3.98 (4 H, m, OCH$_2$), 3.14–3.22 (2 H, m, H-6α, H-2-*exo*), 3.00 (1 H, d, ^3J = 9.0 Hz, H-8), 2.37–2.71 (11 H, m, H-14, H-12, H-13, H-11, H-6β, H-2-*endo*, H-5α), 1.39–1.68 (14 H, m, H-15, H-16, H-17, H-18, H-3, H-4, H-5β, H-7β, H-10), 1.22 (6 H, t, ^3J = 9.0 Hz, CH$_3$), 0.65 (1 H, dd, H-7α). δ_C (75.0 MHz, CDCl$_3$) 150.0 (C-6′), 148.5 (C-4′), 148.2 (C-2′), 130.0 (C-10′), 128.8 (C-8′), 127.5 (C-9′), 126.2 (C-7′), 123.0 (C-3′), 119.3 (C-5′), 77.1 (C-8), 61.5 (C-2), 61.2 (d, $^2J_{C-P}$ = 6.0 Hz, OCH$_2$), 57.3

(C-9), 40.6 (C-6), 34.3 (C-14, d, $^5J_{C–P}$ = 5.3 Hz), 33.0 (C-3), 32.0 (C-13), 31.7 (d, $^3J_{C–P}$ = 15.8 Hz, C-16), 30.2 (C-12), 29.9 (C-11), 29.3 (d, $^2J_{C–P}$ = 17.3 Hz, C-17), 28.8 (C-5), 28.3 (C-7), 26.2 (C-4), 25.4 (d, $^1J_{C–P}$ = 26.2 Hz, C-18), 24.3 (C-10), 21.7 (d, $^4J_{C–P}$ = 4.5 Hz, C-15), 16.1 (d, $^3J_{C–P}$ = 6.0 Hz, CH₃). δ_P (121.0 MHz, CDCl₃) 33.3. Anal. calcd for $C_{30}H_{48}N_3O_3 PS_2$: C, 60.68; H, 8.15; N, 7.08; Found: C, 60.75; H, 8.21; N, 7.01.

Phosphonate 1e. (4.9 g, 76%), brown viscous and oily liquid. δ_H (300 MHz, CDCl₃, Me₄Si) 8.94 (1 H, d, ^3J = 6.0 Hz, H-2′), 8.38 (1 H, d, ^3J = 9.0 Hz, H-5′), 8.17 (1 H, d, ^3J = 9.0 Hz, H-8′), 7.75 (1 H, t, ^3J = 6.0 Hz, H-7′), 7.63 (1 H, t, ^3J = 6.0 Hz, H-6′), 7.58 (1 H, d, ^3J = 6.0 Hz, H-3′), 4.74 (1 H, d, ^3J = 9.0 Hz, H-9), 4.11 (4 H, m, OCH₂), 3.28–3.36 (2 H, m, H-6α, H-2-*exo*), 3.10 (1 H, d, ^3J = 9.0 Hz, H-8), 2.29–2.73 (11 H, m, H-14, H-12, H-13, H-11, H-6β, H-2-*endo*, H-5α), 1.67–1.79 (16 H, m, H-15, H-16, H-17, H-18, H-19, H-7α, H-4, H-5β, H-7β, H-10), 1.34 (6 H, t, ^3J = 9.0 Hz, CH₃), 0.79 (1 H, dd, H-7α). δ_C (75.0 M Hz, CDCl₃) 150.2 (C-6′), 148.5 (C-4′), 148.4 (C-2′), 130.3 (C-10′), 128.9 (C-8′), 127.6 (C-9′), 126.4 (C-7′), 123.1 (C-3′), 119.5 (C-5′), 77.1 (C-8), 61.7 (C-2), 61.2 (d, $^3J_{C–P}$ = 6.8 Hz, OCH₂), 57.4 (C-9), 40.8 (C-6), 34.4 (C-14), 34.2 (C-3), 32.2 (C-13), 32.0 (C-15), 30.1 (C-12), 29.9 (C-16), 29.2 (C-17), 28.4 (C-5), 28.1 (C-7), 26.4 (C-4), 25.4 (d, $^1J_{C–P}$ = 22.5 Hz, C-19), 24.5 (C-10), 22.1 (d, $^2J_{C–P}$ = 4.5 Hz, C-18), 16.3 (d, $^3J_{C–P}$ = 6.0 Hz, CH₃). δ_P (121.0 MHz, CDCl₃) 33.0. Anal. calcd for $C_{31}H_{50}N_3O_3PS_2$: C, 61.25; H, 8.29; N, 6.91; Found: C, 61.31; H, 8.34; N, 6.82.

General procedure for various zirconium phosphonates

Zirconium phosphonates 2a–e. A mixture of phosphonates **1a–e** (4.1 mmol), acetic acid (30 mL) and hydrochloric acid (10 mL, 36%) was stirred at 80 °C for 24 h and concentrated under reduced pressure to 5 mL solution. Then 100 mL of water was added and pH of solution was adjusted to 1–2. To the obtained solution was added dropwise 30 mL of zirconium oxychloride (5.7 g, 17.7 mmol) aqueous solution with stirring and aged at room temperature for another 2 h. The white solids were filtered, dispersed in 50 mL of water and adjusted to pH = 6–7 using NaHCO₃ solution (0.1 mol L^{-1}). The resulting white mud cake was filtered, washed by deionized water (20 mL × 3) until the chloride ion was not detected by ion chromatography, and dried at 60 °C for 12 h under reduced pressure to afford the light yellow zirconium phosphonates **2a–e** (**2a**: 0.71 g, 47%; **2b**: 0.92 g, 56%; **2c**: 1.29 g, 63%; **2d**: 0.79 g, 54%; **2e**: 0.82 g, 42%). C, H and N elemental analysis of **2a–e** are shown in the ESI.†

Zirconium phosphonates 3b and c. A mixture of phosphonate **1b** or **1c** (3.0 mmol), acetic acid (20 mL) and hydrochloric acid (6 mL, 36%) was stirred at 80 °C for 24 h and concentrated to 20 mL solution. Under stirring, 20 mL of ZrOCl₂ aqueous solution (3.7 g, 11.5 mmol) was added dropwise and stirred for another 2 h. The reaction mixture was adjusted to pH = 4–5 with triethylamine aqueous solution (10 wt%), then white solids precipitated. The white solids were filtered, washed with methanol (20 mL × 3) and dried at 50 °C under reduced pressure for 12 h to afford zirconium phosphonates **3b** (0.65 g, 58%) and **c**

(0.72 g, 64%). C, H and N elemental analysis are shown in the ESI.†

Zirconium phosphonate 4c. A mixture of phosphonate **1c** (3.2 g, 5.4 mmol), acetic acid (40 mL) and hydrochloric acid (15 mL, 36%) was stirred at 80 °C for 24 h, concentrated to 10 mL solution and adjusted to pH = 2–3 with aqueous NaHCO₃ solution (0.1 mol L^{-1}). To the reaction mixture was added sodium dodecyl benzene sulfonate (SDBS, 2.0 g in 70 mL 30% THF aqueous solution) and stirred for another 30 min. Then, 25 mL of ZrOCl₂ aqueous solution (6.7 g, 20.6 mmol) was added at room temperature and stirred for 2 h. The precipitate was filtered, washed with water (20 mL × 3) and dried at 60 °C under reduced pressure for 12 h to afford off-white zirconium phosphonate **4c** (1.6 g, 76%).

Hybrid zirconium phosphate–phosphonates 5c₁₋₃. A mixture of phosphonate **1c** (0.2 g, 0.34 mmol), acetic acid (9 mL) and hydrochloric acid (3.0 mL, 36%) was stirred at 80 °C for 24 h, concentrated to 1 mL solution and adjusted to pH = 2–3 by triethylamine aqueous solution (10 wt%). To the resulting solution was added saturated NaH₂PO₄·2H₂O (53 mg, 0.34 mmol) aqueous solution and well mixed. Then, 2 mL of ZrOCl₂ (0.2 g, 0.62 mmol) aqueous solution was added. The amorphous precipitate in the solution was kept at 70 °C for 12 h, cooled to room temperature, filtered, washed with deionized water and dried at 60 °C under reduced pressure to afford white solid **5c₁** (2.2 g, 78%). According to the same procedure mentioned above, hybrid zirconium phosphate–phosphonates **5c₂** (2.1 g, 82%) and **5c₃** (2.1 g, 89%) were also prepared by using the molar ratio of phosphonate/phosphate = 1/2 and 1/3, respectively. C, H and N elemental analysis are shown in the ESI.†

General asymmetric direct aldol reaction. In a 10 mL vial, catalyst **2a** (10 mg, 0.025 mmol) and TfOH (3.75 μmol), water (1 mL) and cyclohexanone (0.5 mL, 3.9 mmol) were added consecutively. After stirred at room temperature for 15 min in a closed system, *p*-nitrobenzaldehyde (37.3 mg, 0.25 mmol) was added and left under stirring for 96 h at 25 °C (monitored by TLC). The reaction mixture was quenched with saturated ammonium chloride solution (5 mL) and extracted with ethyl acetate (15 mL × 3). Then catalyst **2a** was recovered by centrifugation. The combined organic phases were dried over anhydrous Na₂SO₄ and evaporated under reduced pressure. The crude products were purified by flash column chromatography eluting with petroleum ether/ethyl acetate (v/v = 10/1) to remove the unreacted *p*-nitrobenzaldehyde and then petroleum ether/ethyl acetate (v/v = 2/1) as an eluent to afford the pure aldol adduct.

The *anti*/*syn* ratio was determined by ^{1}H NMR of crude product in CDCl₃; CHOH (*d*): *syn* 5.48 ppm, J = 3.0 Hz; *anti*: 4.90 ppm, J = 9.0 Hz. The enantiomeric excess (%ee) was determined by chiral HPLC analysis with CHIRALPACK AD-H, eluting with *n*-hexane/isopropanol (80/20), flow rate 0.5 mL min^{-1} and UV detector (λ = 254 nm).

$$\%\text{ee } anti = \frac{[SR] - [RS]}{[RS] + [SR]} \times 100\%;$$

$$\%\text{ee } syn = \frac{[SS] - [RR]}{[RR] + [SS]} \times 100\%$$

Table 1 Thermal properties and chemical compositions of various supported organocatalysts[a]

Cat.	n	Molecular formula	Weight loss (TG)	
			<150 °C	150–800 °C
2a	2	$Zr(OH)_{3.18}(O_3PR)_{0.41} \cdot 1.98H_2O$	9.0	40.3
2b	3	$Zr(OH)_{3.14}(O_3PR)_{0.43} \cdot 1.76H_2O$	8.0	42.0
2c	4	$Zr(OH)_{2.88}(O_3PR)_{0.56} \cdot 2.89H_2O$	11.8	48.7
2d	5	$Zr(OH)_{3.26}(O_3PR)_{0.37} \cdot 2.02H_2O$	9.3	39.7
2e	6	$Zr(OH)_{3.04}(O_3PR)_{0.48} \cdot 2.28H_2O$	3.0	51.0
3b	3	$Zr(OH)_{3.18}(O_3PR)_{0.41} \cdot 1.12H_2O$	—	—
3c	4	$Zr(OH)_{3.22}(O_3PR)_{0.39} \cdot 1.47H_2O$	6.7	42.4
4c	4	$Zr(OH)_{3.12}(O_3PR)_{0.44} \cdot 1.41H_2O$	5.8	45.2
5c$_1$	4	$Zr(O_3POH)_{1.71}(O_3PR)_{0.29} \cdot 2.14H_2O$	11.2	24.4
5c$_2$	4	$Zr(O_3POH)_{1.78}(O_3PR)_{0.22} \cdot 1.54H_2O$	16.9	18.5
5c$_3$	4	$Zr(O_3POH)_{1.81}(O_3PR)_{0.19} \cdot 1.21H_2O$	12.4	15.6

[a] Zirconium(IV) and phosphonic acid were determined by quantitative colorimetric assay and solution ^{31}P {^1H} NMR respectively; the content of water was determined by TG.

Results and discussion

Catalyst preparation and characterization

Catalyst preparation. The preparation of zirconium phosphonate is closely related to the methods employed for layered α-Zr (HPO$_4$)$_2 \cdot$H$_2$O (α-ZrP), for example, by precipitation of aqueous solutions of phosphonic acids **1a–e** with ZrOCl$_2$ in the absence of hydrofluoric acid. In general, compared with crystalline zirconium phosphonate, amorphous materials obtained by direct precipitation in the absence of hydrofluoric acid showed the better catalytic properties in the field of catalysis, such as hydrogenation reactions, owing to much higher surface area.[23] In this paper, we only paid attention to the preparation of amorphous zirconium phosphonates by direct precipitation upon adding ZrOCl$_2$ to the aqueous solution of phosphonic acid (Zr^{IV}/P = 4). Due to the limited free area (24 Å^2) around each phosphorous atom and steric effect of attached bulky organic moiety on the surface of Zr layer, typical zirconium phosphonate with molar ratio of P/Zr = 2, whose theoretical formula is considered to be Zr(O$_3$PR)$_2 \cdot n$H$_2$O (R being an organic group), cannot be obtained as expected. However, bulky groups can be attached to the Zr layer to afford functional compounds of the formula Zr(O$_3$PR)-(O$_3$PR′)$\cdot n$H$_2$O if their dimensions are compensated by introducing a small group, such as R′ = H, OH or CH$_3$. Otherwise, in the presence of a sole bulky phosphonate without a small compensating group, zirconium hydroxide phosphonates of the formula Zr(OH)$_{4-2x}$(O$_3$PR)$_x \cdot n$H$_2$O can be prepared by direct precipitation with ZrOCl$_2$ solution.[21d,22a]

Ethyl phosphonates **1a–e** with different chain lengths (n = 2–6) can be hydrolyzed at 80 °C in HOAc/HCl medium to form corresponding alkyl phosphoric acids, which were chosen *in situ* for the preparation of zirconium hydroxide phosphonate-covalently supported 9-amino-9-deoxy-*epi*-cinchonine organocatalysts **2a–e** in 40–50% yields. Considering the effect of internal and external surface properties of zirconium phosphonate on catalytic properties, Et$_3$N and SDBS were used as template guest molecules to prepare zirconium phosphonates **3b, c** and **4c**, respectively, because amine and surfactant played important roles in different microtextures and surface morphologies of zirconium phosphonate. Apart from acting as charge balancing cations, amine and surfactant can act in three distinct ways: (1)

as space-filling species, (2) as structure-directing agents, and (3) as true templates.[24] Meanwhile, upon introducing a small group, such as HPO$_4$, hybrid zirconium phosphate–phosphonates **5c$_1$–c$_3$** of general formula Zr(HPO$_4$)$_{2-x}$(PO$_3$R)$_x$ (x = 0.29, 0.22 and 0.18) were also prepared as amorphous solids by direct precipitation in the absence of hydrofluoric acid (Scheme 1). They were all characterized by TG, DTA, X-ray, nitrogen adsorption–desorption isotherm, AFM and TEM.

Chemical composition. F$^-$ is a good ligand for transitional metals, such as zirconium(IV), with a very high oxidation state. Upon adding 2 mL of hydrofluoric acid (30%) and 2 mL of deionized water to zirconium phosphonates **2a–e** (50 mg) and stirring for 6 h at room temperature in a sealed plastic container, **2a–e** were decomposed to the water-soluble mixtures of complex ZrF$_6^{2-}$ and organophosphonic acid. The contents of zirconium (IV) and organophosphonic acid in the resulting solution could be determined by quantitative colorimetric assay and solution ^{31}P {^1H} NMR, respectively. Based on the detected molar ratio of Zr/P, the x values in empirical formulae of **2a–e** [Zr(OH)$_{4-2x}$-(O$_3$PR)$_x \cdot n$H$_2$O, R = organic group] were calculated to be 0.41, 0.43, 0.56, 0.37 and 0.48, respectively (Table 1), which were in good agreement with the results of elemental analysis. On the other hand, the molecular formulae of **2a–e**, whose x values were 0.39, 0.40, 0.54, 0.35 and 0.47, were also evaluated by TGA. However, due to the incomplete combustion, which is suggested by the typical pale gray color of the residue after TGA, led to a somewhat reduced weight loss and a minor under-prediction of the x values. To elucidate the effect of template molecules Et$_3$N and SDBS on the amount of appended phosphonate (x), ethyl phosphonate **1c** was used as a representative example to prepare corresponding zirconium phosphonates **3b, c** and **4c**. Compared with zirconium phosphonate **2c**, the organic weight losses of **3c** and **4c** surprisingly decreased from 48.7% (x = 0.56) to 42.4 (x = 0.39) and 45.2% (x = 0.44), respectively. By means of introducing a small compensating group HPO$_4$ in the presence of NaH$_2$PO$_4$, amorphous organic–inorganic hybrid zirconium phosphonates **5c$_1$–c$_3$** of molecular formulae [Zr(HPO$_4$)$_{2-x}$-(PO$_3$R)$_x$] with x = 0.29, 0.22 and 0.18 can be obtained, respectively, by the direct precipitation of the mixture of hydrolytic organophosphonate **1c** and NaH$_2$PO$_4$ (molar ratio NaH$_2$PO$_4$/**1c** = 1, 2 and 3)

with ZrOCl$_2$ (Zr^{IV}/P = 2) in the absence of hydrofluoric acid (Table 1).

From the TG curves, it was observed that thermal decomposition occurred in two steps: the first, between 50 and 150 °C, corresponded to the initial weight losses of 11.8, 6.7, 5.8 and 11.2% owing to the surface-bound or intercalated water absorbed in pores; the second, between 150 and 800 °C, corresponded to the total weight losses of 48.7, 42.4, 45.2 and 24.4% of the initial and deep decomposition of appended organic fragments, respectively (Fig. S1 in ESI†).

The covalent attachment of 9-amino-9-deoxy-*epi*-cinchonine on the frame of zirconium phosphonate was also successfully verified by infrared spectra in the range of 4000–400 cm^{-1} (Fig. S2 shown in ESI†). The broad, strong and wide absorption band extending from 3700–2500 cm^{-1} and centered at 3450 cm^{-1} was assigned to the O–H stretching vibration, which was indicative of the presence of hydrogen bonds between hydroxyl groups or adsorbed waters on the internal and external surfaces. The moderate absorption bands at 1641, 1610, and 623 cm^{-1} were attributed to the stretching vibration mode and flexural vibration of the aryl group, respectively. The flexural vibration of C–H in CH$_2$ groups, which emerged at 1398 cm^{-1}, was strengthened with the increase in arm chain length (*n*) from 2 to 6. The strong and wide absorption band at about 1091 cm^{-1} was caused by the characteristic Zr–O–P stretching vibration.[25]

Layered and porous structure. The layered structure and *d*-spacing of zirconium planes for crystalline and semi-crystalline zirconium phosphonate can be determined from the 00*n* peak in powder XRD pattern (*via* the Bragg equation, $n\lambda = 2d\sin\theta$). The X-rays of zirconium phosphonates **2a–e** and **3b–c** showed the amorphous nature with the broad peak, which illustrated that they possessed layered structures with different interlayer distances: 4.5–5.0 Å typical of Zr(OH)$_{4-2x}$ phase and 15.8–25.7 Å typical of Zr(O$_3$PR)$_x$ phase arose from the packing of alternate layers with different interlayer distances, one richer in hydroxide (OH) and the other in phosphonate (O$_3$PR), respectively. With the increase of arm chain length (*n*) from 2 to 6, the typical interlayer distances of **2a–e** [Zr(OH)$_{4-2x}$-

(O$_3$PR)$_x$·*n*H$_2$O] consecutively increased from 15.8 to 16.3, 16.7, 20.8 and 25.7 Å (Fig. S3 shown in ESI†). Preliminary attempts had been made to estimate the effect of template guest molecules, such as Et$_3$N, on interlayer distances. Interestingly, it was found that the typical interlayer distances of **3b, c** were expanded to 19.0 and 19.9 Å with 2.7 and 3.2 Å increments, respectively.

In Table 2 were listed, for all as-synthesized zirconium phosphonates **2a–e**, **3b–c**, **4c** and **5c**, the arm chain length (*n*), molecular formula, typical interlayer distance, BET-specific surface area, average pore diameter and pore volume by BJH analysis. As a pair of representative and comparative examples, the nitrogen adsorption–desorption isotherm plots of **2c** and **3c**, performed at 77 K, were shown in Fig. 1. Unusually, the isotherm plots of **2a–e** were linear to the P/P_0 axis at relative low P/P_0 range (0–0.9) and convex to the P/P_0 axis at high P/P_0 range (0.9–1.0), which were beyond to classic definitions.[26] From the calculated data in Table 1 and Fig. 1, these pore size distributions (PSDs) of as-synthesized **2a–e** suggested the existence of 10–20 nm micropores together with irregular mesopores, having

Table 2 The layered and mesoporous properties of as-synthesized zirconium phosphonates[a]

Cat.	*n*	Surface area[b] (m^2 g^{-1})	Average pore diameter[c] (Å)	Pore volume[d] (×10^{-3} cc g^{-1})	Interlayer distance (Å)
2a	2	12.6	50.4	32.1	4.5, 15.8
2b	3	16.3	50.0	38.4	4.7, 16.3
2c	4	28.1	52.0	43.0	4.8, 16.7
2d	5	29.9	55.8	38.8	4.9, 20.8
2e	6	33.2	57.8	38.2	5.0, 25.7
3b	3	16.5	58.0	19.7	4.7, 19.1
3c	4	12.8	59.8	18.6	5.0, 19.9
4c	4	16.2	53.0	43.2	5.1, 19.8
5c$_1$	4	32.1	94.2	71.8	7.8, 19.2
5c$_2$	4	30.1	91.8	78.3	—
5c$_3$	4	30.4	94.3	143.2	—

[a] The sample was degassed at 100 °C for 5 h. [b] Based on multipoint BET method. [c] Based on the desorption data using BJH method. [d] Based on the desorption data of BJH method.
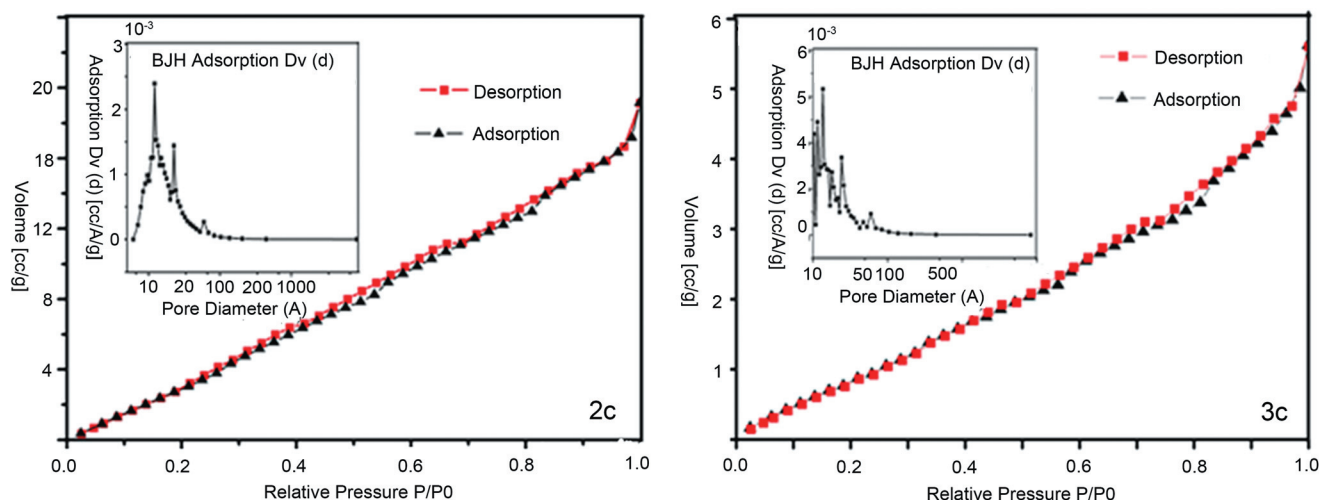

Fig. 1 Nitrogen adsorption–desorption isotherm plots obtained with catalysts **2c** and **3c**.
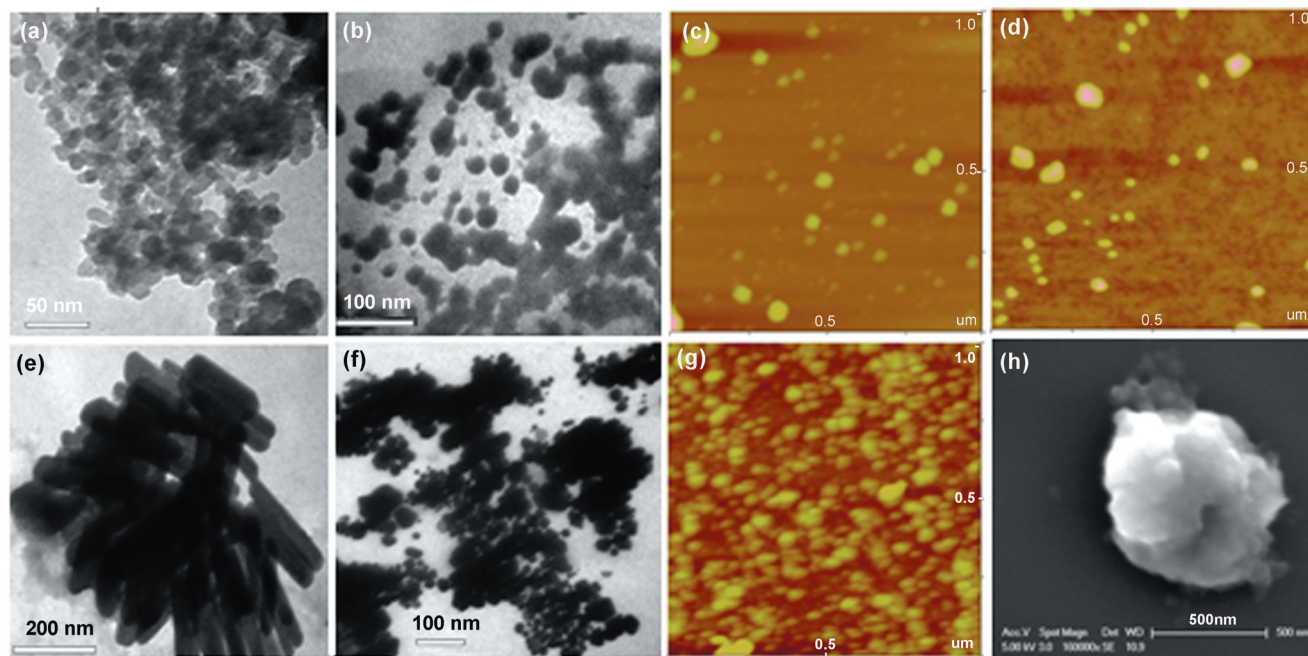
Fig. 2 (a) TEM image of **2b**; (b) TEM image of **2c**; (c) AFM image of **3c**; (d) AFM image of **4c**; (e) TEM image of **5c₁**; (f) TEM image of **3c**; (g) AFM image of **5c₁**; (h) SEM image of **3c**.

broad peaks in the range of about 2–50 nm. As expected, the average pore diameters and surface areas of **2a–e** increased from 50.4 to 57.8 Å and 12.6 to 33.2 $m^2\ g^{-1}$, respectively, with the increase of arm chain length (n) from 2 to 6. Unfortunately, the as-synthesized zirconium phosphonates **2a–e** presented the low pore volumes (18.6–$43.0 \times 10^{-3}\ cc\ g^{-1}$). Upon adding template guest molecule (Et_3N), the surface areas (16.5 and $12.8\ m^2\ g^{-1}$) and pore volumes (19.7 and $18.6 \times 10^{-3}\ cc\ g^{-1}$) of zirconium phosphonates **3b, c** decreased by 20 and 57%, respectively, except for a little increase of average pore diameters ($50.0 \rightarrow 58.0$ Å and $52.0 \rightarrow 59.8$ Å, respectively). Surface-active agent (SDBS) showed no pronounced change in average pore diameter and pore volume of zirconium phosphonate **4c**. After introducing a small HPO_4 group, the hybrid zirconium phosphate–phosphonates **5c₁–c₃** possessed higher surface areas, average pore diameters and pore volumes owing to their rigid and classic skeleton construction.

Surface morphology. Taking into account the compact relationship between the physical surface properties of a supported catalyst and its catalytic performance, it was necessary that zirconium phosphonates **2a–e**, **3b, c**, **4c**, **5c** be well elucidated by SEM, TEM and AFM to understand surface morphologies and particle sizes in different states. After being well-dispersed in water (10 mg sample in 10 mL of H_2O) for 10 min under ultrasonic radiation, sputtered over copper wire, and evaporated under infrared radiation for 10 min, the TEM images were observed under an accelerating rate voltage of 200 keV. From Fig. 2 as representative and comparative examples, the spherical particles **2b** and **2c** in water, with a uniform diameter of approximately 20–30 nm, were observed, and the spherical particles closely connected to each other to form the filiform structure. As expected, upon adding NaH_2PO_4, the surface morphology of **5c₁**

with about 200 nm length and 20 nm width was directly evidenced by TEM image, which was similar to that of typical crystalline particles. Interestingly, compared with zirconium phosphonate **2c**, it is worth noting that zirconium phosphonate **3c** apparently became smaller in size and more regular in shape owing to the action of template guest molecule (Et_3N). From the TEM images (Fig. 2a, b, e and f), it was concluded that the different surface morphologies could be obtained by using different template guest molecules.

AFM was also used to observe the morphologies and particle sizes in water. The samples were prepared as follows: 1.0 mg of particles was dispersed in 3 mL of water, followed by ultrasonic stirring for 10 min. A thin film of the suspension on mica was prepared by spin coating, and the particles were left on the mica surface after volatilization of water for three days. The two-dimensional AFM images of zirconium phosphonates **3c**, **4c** and **5c₁** were shown in Fig. 2c, d and g, and the three-dimensional AFM images were shown in the ESI.† Among the statistically analyzed 29 particles for zirconium phosphonate **3c**, the diameter and height ranged from 4.4–95.5 nm and 4.0–22.1 nm with 33.8 nm mean diameter and 8.1 nm mean height, respectively. Similar results with 39.9 nm mean diameter and 10.2 nm mean height were also observed for zirconium phosphonate **4c**. For hybrid material **5c₁**, 142 particles were statistically analyzed and the smaller mean diameter (23.1 nm) and height (4.0 nm) were obtained in aqueous medium.

Seen from the outside, it seemed to be a contradiction among SEM, TEM and AFM images. In fact, they clearly reflected the different surface morphologies of zirconium phosphonate in different states. The SEM image with about 500 nm, which was observed in the solid state, could be considered to mirror the surface morphology of catalyst in solid state. Due to being well-dispersed in water, the TEM and AFM images could be

identified as efficiently elaborating the surface morphologies of zirconium phosphonate in aqueous solution, which seemed to simulate the existing state of zirconium phosphonate in water in aldol addition. It was worthy noting that the smaller particle sizes and being more homogeneously dispersed were observed by using AFM images owing to the more diluted solution (0.3 mg mL^{-1}).

Catalytic activity

In particular, the asymmetric aldol reaction is a key C–C bond-forming reaction that has tremendous synthetic utility and is often the platform of choice to examine new organocatalysts. There are a number of small molecule-organocatalyzed aldol reactions that are capable of asymmetric induction in organic solvents. However, from a green chemistry perspective, the use of water instead of organic solvent and the reuse of organocatalyst are preferred to decrease environmental contamination and lower the cost of the organocatalyst.[27] For the above-mentioned reasons, we draw attention to particular aspects of developing asymmetric aldol reactions in water and the recycling of small-molecule organocatalyst owing to striving for environmentally benign chemical processes and economic benefits. Zirconium phosphonate, a kind of widely recognized porous and layered materials with accessible channels as well as good thermal and hydrothermal stability, was applied as a support for 9-amino-9-deoxy-*epi*-cinchonine in this work. The aldol addition of *p*-nitrobenzaldehyde to cyclohexanone to give *anti* and *syn* diastereomers of 2-[hydroxy(4-nitrophenyl)methyl]cyclohexanone was chosen as a model reaction for evaluating the asymmetric catalytic performances of various zirconium phosphonates-supported organocatalysts.

The influence of arm chain lengths (*n*) and different preparation conditions. Our initial experiments were performed using *p*-nitrobenzaldehyde as a model substrate with cyclohexanone over 10 mol% **2a–e** with different organic arm chain lengths (*n* = 2–6) at 25 °C for 96 h in water. It was exciting to observe that the corresponding aldol adducts in 75–98% isolated yields with 80–88%ee *anti*, 19–42%ee *syn* and about *anti*/*syn* = 70/30 were favorably obtained in the presence of 1.5 mol% triflic acid (Table 3, entries 1–5). With the increase of arm chain length (*n*) from 2 to 6, the yields and enantioselectivities of *anti*-aldol adducts were gradually enhanced first (75 → 98% and 82 → 88%ee *anti*), then decreased at *n* = 5 (98 → 82% and 88 → 80%ee *anti*). This phenomenon was possibly related to the different confinement effects of the backbones in **2a–e** owing to the arm chain lengths (*n*), in which 9-amino-9-deoxy-*epi*-cinchonine moiety possessed the different distances from Zr layers (Fig. 3). The optimum arm chain length was found to be *n* = 4 in terms of enantioselectivity, diastereoselectivity and reactivity (98% yield, 88%ee *anti*) (Table 3, entry 3). Too far or too near from the Zr layer was not beneficial to the confinement effect of zirconium phosphonate. Moreover, it was worth noting that the successively enhanced enantioselectivities (20 → 42%ee) and similar dr values (*anti*/*syn* = 70/30) of *syn*-adducts were observed with the increase of arm chain lengths (*n*) from 2 to 6.

The sole difference in synthetic procedure between **2a–e** and **3b, c** was using inorganic base NaHCO$_3$ or organic base Et$_3$N to

Table 3 The direct asymmetric aldol reaction of *p*-nitrobenzaldehyde and cyclohexanone over various zirconium phosphonates in water[a]

Entry	Cat.	*n*	Yield[b] (%)	*Anti*-product[c] (%ee)	*Syn*-product[c] (%ee)	Dr (*anti*/*syn*)[d]
1	**2a**	2	75	82	22	70/30
2	**2b**	3	94	83	20	68/32
3	**2c**	4	98	88	21	70/30
4	**2d**	5	90	85	30	67/33
5	**2e**	6	82	80	42	71/29
6	**3b**	3	98	92	23	77/23
7	**3c**	4	99	95	26	81/19
8	**4c**	4	91	70	30	85/15
9	**5c$_1$**	4	92	91	25	73/27
10	**5c$_2$**	4	75	85	25	63/37
11	**5c$_3$**	4	70	82	9	64/36
12	—[e]		97	99	22	84/16

[a] Reaction conditions: *p*-nitrobenzaldehyde (0.25 mmol), cyclohexanone (0.39 mmol), catalyst (0.025 mmol, 10 mol%), 25 °C, 96 h, 1 mL of water, TfOH (3.75 × 10^{-3} mmol). [b] Isolated yield. [c] Determined by chiral HPLC, Daicel Chiralpak AD-H column. [d] Determined by ^{1}H NMR. [e] 9-Amino-9-deoxy-*epi*-cinchonine as "blank" reaction.
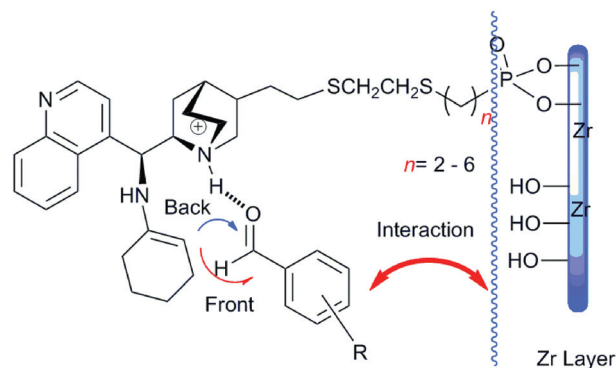

Fig. 3 The possible mechanism of the asymmetric aldol reaction in the confined backbone of zirconium phosphonate.

neutralize the surface acidity of zirconium phosphonates. To our surprise, although the decrease in the *x* value, surface area and pore volume for **3c**, based on TGA and nitrogen adsorption–adsorption isotherms, was observed, the enantioselectivities (88 → 95%ee) and diastereoselectivities (70/30 → 81/19) of aldol adducts were remarkably improved (Table 3, entries 6 and 7). Perhaps, the improvement of catalytic performance could be attributed to the acid–base reaction between the organic base Et$_3$N and the surface acid of the hydroxyl over the zirconium layer to form triethylamine hydrochloride and result in the change in surface morphology evidenced by TEM (Fig. 2). Unfortunately, upon adding template guest molecule SDBS in the synthetic procedure of zirconium phosphonate **4c**, the %ee of *anti*-products dropped significantly but the dr value unexpectedly increased for reasons unknown (Table 3, entry 8). It was noteworthy that hybrid zirconium phosphonate **5c$_1$** (*x* = 0.29)
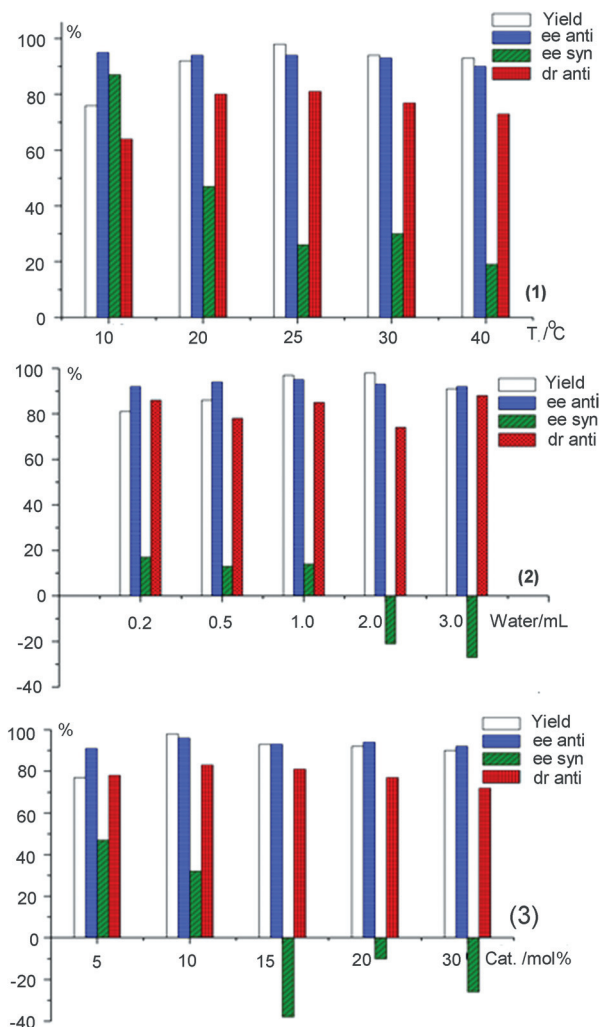
Fig. 4 The effects of temperature and amounts of water and catalyst used on the catalytic properties.

with the cylindrical morphology showed that the good catalytic activity (92% yield) and enantioselectivity (91%ee *anti*, *anti/syn* = 73/27) (Table 3, entry 9) were also achieved. However, **5c₂** and **5c₃** gave more and more disappointing results in the catalytic properties along with the decrease in the *x* values (0.29 → 0.19) of appended 9-amino-9-deoxy-*epi*-cinchonine determined by TGA (Table 3, entries 10 and 11), although they possessed higher surface areas, average pore diameters and pore volumes (Table 2). In conclusion, the preliminary investigation showed that the synthetic conditions played an important role in the microtexture and surface morphology of zirconium phosphonate, which resulted in different catalytic results in the asymmetric aldol addition in water.

The influence of temperature and used amount of water and catalyst. In order to further improve the catalytic activity of zirconium phosphonate **3c**, we investigated the effect of temperature and used amount of water and catalyst on reactivity and selectivity in the presence of 1.5 mol% triflic acid (Fig. 4). Lowering the reaction temperature to 10 °C, the reactivity decreased to 76% yield. However, the higher 97%ee *anti*-adduct and 87%

Table 4 The direct asymmetric aldol addition of benzaldehyde derivatives to cyclohexanone in water[a]

Entry	R	Yield[b] (%)	*Anti*-product[c] (%ee)	*Syn*-product[c] (%ee)	Dr (anti/syn)[d]
1	2-NO₂	81	20	−90	1/99
2[e]	2-NO₂	83	95	−44	98/2
3	3-NO₂	90	94	7	90/10
4[e]	3-NO₂	98	98	36	86/16
5	4-NO₂	98	96	32	83/17
6[e]	4-NO₂	97	99	22	84/16
7	4-CN	86	94	32	74/26
8	4-F	11	94	47	77/23
9	4-Cl	47	91	−53	95/5
10	4-Br	14	93	66	82/18
11	4-CH₃	15	86	34	78/22
12	4-OCH₃	12	94	28	68/32
13	H	30	5	−63	90/10

[a] Reaction conditions: Benzaldehydes (0.25 mmol), cyclohexanone (0.39 mmol), catalyst **3c** (0.025 mmol, 10 mol%), 25 °C, 96 h, 1 mL of water, TfOH (3.75 × 10⁻³ mmol). [b] Isolated yield. [c] Determined by chiral HPLC (Daicel Chiralpak AD-H column). [d] Determined by ¹H NMR. [e] 9-Amino-9-deoxy-*epi*-cinchonine as "blank" reaction (25 °C, 6 h).

ee *syn*-adduct were obtained. In the relatively high temperature range from 25–40 °C, the %ee *anti* dropped successively and slightly from 96 to 90%ee, and the %ee *syn* fell badly from 87 to 19%ee without significant change in the reactivities (93–98%) and diastereoselectivities (*anti/syn* = 80/20) (Fig. 4-1). The best result was obtained at 25 °C in 1 mL of water per 0.25 mmol of *p*-nitrobenzaldehyde with excellent conversion (98% yield) and high stereoselectivity (*anti/syn* = 81/19, 96%ee *anti*). Fig. 4-2 showed the catalytic properties of supported organocatalyst **3c** as a function of the used H₂O volume. At the lower used amount of water, a strong inhibiting influence on the yields of aldol adducts (0.2 mL, 81%; 0.5 mL, 86%) was clearly observed owing to the poorer mass diffusion in the mesopores of supported organocatalyst **3c**. Of particular note was that at the higher used amounts of H₂O volume (2 and 3 mL), the %ee of aldol *syn*-adducts changed from a positive value (major *S,S*-configuration) to a negative value (major *R,R*-configuration). The same phenomenon was also observed in the catalytic process using the higher amounts of catalyst (>15 mol%) (see Fig. S8 in ESI†). Therefore, we conjectured that, at low substrate concentration (<0.03 mol L⁻¹) or high used amount of catalyst (>15 mol%), the reactants in the mesopores of catalyst **3c** were considered to be in the diluted state, and in such a state the *re*-facial attack on arylaldehyde to form the *R,R*-configuration was favored owing to steric confinement. In conclusion, the optimum and excellent catalytic properties (98% yield, 96%ee *anti* and 83/17 dr) were obtained by using 10 mol% **3c** at 25 °C in 1 mL water for 96 h (Fig. 4-3).

Confinement effect of zirconium phosphonate. The optimized protocol was expanded to a wide variety of benzaldehydes (Table 4). The results of these trials indicated that the aldol

reaction was dramatically dependent on the electronic effect of the substituents similar to proline and its derivatives. 4-, 3-, 2-Nitrobenzaldehydes and 4-cyanobenzaldehyde with electron-drawing groups at the aromatic ring underwent asymmetric aldol addition smoothly with cyclohexanone in good to excellent yields (81–98%), excellent enantioselectivities (90–96%ee) and diastereoselectivities (*anti/syn* = 1–90/99–26) (Table 4, entries 1, 3, 5, 7). However, unsubstituted benzaldehyde was less reactive and afforded the aldol adducts in 30% yield with −63%ee *syn* and good *anti/syn* = 90/10 (Table 4, entry 13). Meanwhile, the substituted benzaldehydes with halogen groups (X = 4-F, Cl and Br) and electron donating groups, such as CH_3 and OCH_3, at the aromatic ring were not suitable for aldol addition in 11–47% yield and 86–94%ee *anti* (Table 4, entries 8–13).

In the reported asymmetric homogeneous aldol addition of substituent nitrobenzaldehydes to cyclohexanone, whether the nitro substituent was in the *o*-, *m*- or *p*- position of the aromatic ring, the major product of aldol addition had (2S,1′R) absolute stereochemistry.[8c,28] However, it was worth noting that the stereoselectivities of aldol adducts catalyzed by heterogeneously supported organocatalyst **3c** were extremely related to the *o*-, *m*-or *p*-position of the substituent (NO_2) at aromatic ring (Fig. 5). Especially, when the nitro substituent group was at the *ortho*-position of benzaldehyde, the major *syn*-aldol adduct with good −90%ee and excellent *anti/syn* = 1/99 were obtained. This phenomenon was never observed in the homogeneous catalysis of 9-amino-9-deoxy-*epi*-cinchonine (Table 4, entry 1). Under the same catalytic conditions, *m*-nitrobenzaldehyde afforded (2S,1′R)-configuration with 94%ee *anti* and *anti/syn* = 90/10 (Table 4, entry 3), and the same (2S,1′R)-configuration was also achieved by *p*-nitrobenzaldehyde in 98% yield, 96%ee *anti* and *anti/syn* = 83/17 (Table 4, entry 5). For *m*- and *p*-nitrobenzaldehydes, their stereoselectivities were in accordance with the results catalyzed by homogeneous 9-amino-9-deoxy-*epi*-cinchonine (Table 4, entries 4, 6). Based on the different stereochemical results in homogeneous and heterogeneous catalysis, we speculated that, in the confined pores of zirconium phosphonate, the different steric strains caused by the steric interactions between the *o*-position of nitro substituent and the backbone of **3c** made planar nitrobenzaldehyde in different steric direction, and resulted in the apofacial or facial attack to form the different configurations (Fig. 3). The further mechanistic understanding involving both experimental and complementary computational exploration is under detailed investigation.

The recovery and reuse of catalyst

At the end of the catalytic aldol reaction, zirconium phosphonate **3c** was readily recovered from the reaction mixture by simple centrifugal separation, washed with ethyl acetate and reused without any other further treatment. To our disappointment, the catalytic activity was observed to have a sharp decline, even at the first run (Table 5, entries 1–4). To make clear what is responsible for the sharp decease in the catalytic activity, the supported organocatalyst **3c** was stirred in 10 mL of 30 wt% Et_3N aqueous solution for 15 min in every recycle run, centrifuged and dried in a vacuum. It is exciting that the 88% yield, 91%ee *anti* and *anti/syn* = 78/22 were still observed, even in the fifth run
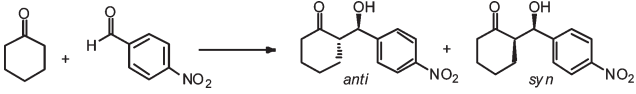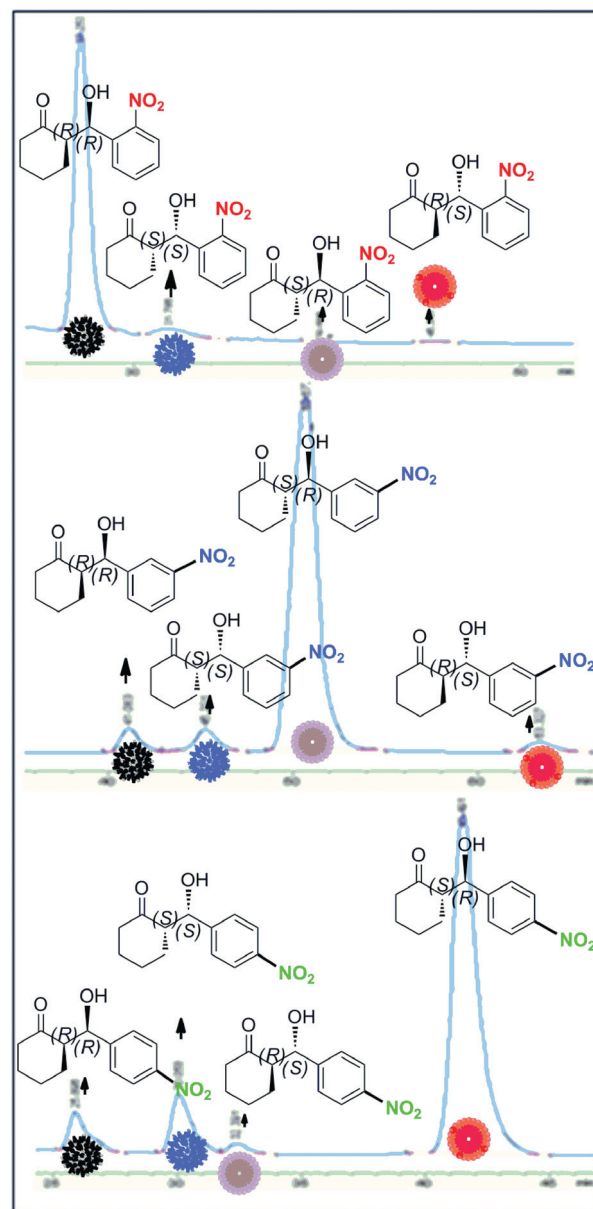

Fig. 5 Stereoisomers determined by HPLC in the aldol reaction of *o*-, *m*-, or *p*-nitrobenzaldehydes with cyclohexanone.

(Table 5, entry 9), although there was appreciable drop in the yield (8%) and enantioselectivity (4%ee *anti*). In order to seek the reason why the catalytic activity decreased slightly, TEM, TGA and nitrogen adsorption–desorption isotherm were used to monitor the surface morphology, weight percent of organic moiety and pore structure of the recycled catalyst **3c** in the fifth run (Fig. 6). Compared with fresh catalyst **3c**, the similar spherical particles with a uniform diameter of approximately 20–30 nm were also observed. However, it was found that the organic weight loss of organic moiety in the temperature range of 150–800 °C increased from 42.4 to 65.9% and the average pore diameter sharply decreased from 59.8 to 5.9 Å, which implied that the adsorbed reactants, products, or impurity occupied some pores, covered the catalytic active sites and resulted in the decrease in catalytic activity.

Table 5 The direct asymmetric aldol addition of *p*-nitrobenzaldehyde to cyclohexanone over the recycled zirconium phosphonate **3c** in water[a]

Entry	Recycle run	Yield[b] (%)	Anti-product[c] (%ee)	Syn-product[c] (%ee)	Dr (anti/syn)
1	1[d]	95	95	36	80/20
2	2[d]	91	82	34	56/44
3	3[d]	83	78	38	55/45
4	4[d]	80	72	30	55/45
5	1[e]	95	96	38	88/12
6	2[e]	96	94	40	78/22
7	3[e]	91	95	32	77/23
8	4[e]	90	92	37	77/23
9	5[e]	88	91	12	78/22

[a] Reaction conditions: *p*-nitrobenzaldehyde (0.25 mmol), cyclohexanone (0.39 mmol), catalyst **3c** (0.025 mmol, 10 mol%), 25 °C, 96 h, 1 mL of water, TfOH (3.75×10^{-3} mmol). [b] Isolated yield. [c] Determined by chiral HPLC, Daicel Chiralpak AD-H column. [d] Washed with ethyl acetate. [e] Washed with Et$_3$N.
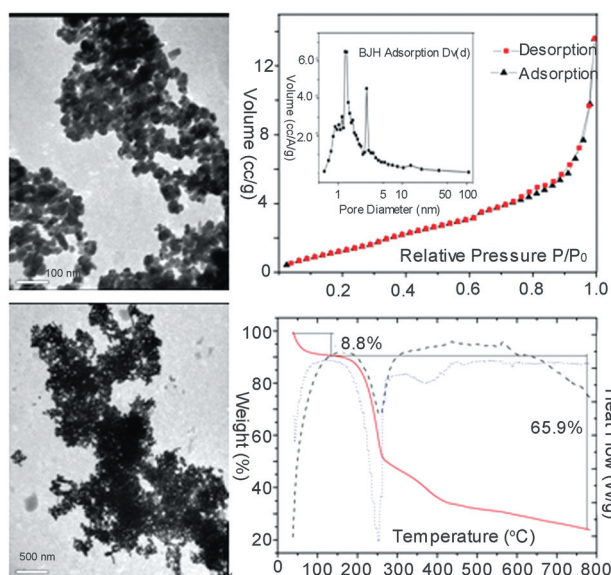

Fig. 6 The TEM images, TGA and nitrogen adsorption–desorption isotherm of recycled catalyst **3c** in the fifth run.

Conclusions

In this work, we reported the preparation and characterization of novel amorphous zirconium phosphonates with different arm chain lengths ($n = 2$–6) by the covalent attachment of 9-amino-9-deoxy-*epi*-cinchonine, which can be readily used as heterogeneous organocatalysts in asymmetric aldol addition. The best feature was that those heterogeneous organocatalysts with excellent catalytic properties were used in aqueous medium, and could be readily recycled by simple centrifugation and regenerated by 30 wt% aqueous Et$_3$N without significant loss of catalytic activity. In addition, the confinement effect as well as the

accessibility of reactants in the mesopores played an important role in determining the configuration and enantiomeric excess among the four stereo-isomers in the asymmetric aldol addition of nitrobenzaldehyde to cyclohexanone. Based on this phenomenon, the relationship between the structure and its catalytic property of catalyst is under the further investigation in detail in our lab by tuning the pore structure and tailoring the conformation of 9-amino-9-deoxy-*epi*-cinchonine in various metal phosphonates (M = Zr, Ti, Ni, Zn and Ga).

Notes and references

1 (*a*) B. M. Trost and C. S. Brindle, *Chem. Soc. Rev.*, 2010, **39**, 1600–1632; (*b*) G. Casiraghi, L. Battistini, C. Curti, G. Rassu and F. Zanardi, *Chem. Rev.*, 2011, **111**, 3076–3154; (*c*) F. B. Chen, S. Huang, H. Zhang, F. Y. Liu and Y. G. Peng, *Tetrahedron*, 2008, **64**, 9585–9591; (*d*) W. B. Zou, P. Dziedzic, I. Ibrahem, E. Reyes and Y. M. Xu, *Chem.–Eur. J.*, 2006, **12**, 5383–5397; (*e*) L. M. Geary and P. G. Hultin, *Tetrahedron: Asymmetry*, 2009, **20**, 131–173.

2 (*a*) T. Miura, K. Imai, H. Kasuga, M. Ina, N. Tada, N. Imai and A. Itoh, *Tetrahedron*, 2011, **67**, 6340–6346; (*b*) Y. W. Zhu, W. B. Yi and C. Cai, *J. Fluorine Chem.*, 2011, **132**, 71–74; (*c*) L. S. Zu, H. X. Xie, H. Li, J. Wang and W. Wang, *Org. Lett.*, 2008, **10**, 1211–1214; (*d*) F. Fache and O. Piva, *Tetrahedron: Asymmetry*, 2003, **14**, 139–143.

3 (*a*) S. Calogero, D. Lanari, M. Orrù, O. Piermatti, F. Pizzo and L. Vaccaro, *J. Catal.*, 2011, **282**, 112–119; (*b*) M. Portnoy and T. Kehat, *Chem. Commun.*, 2007, 2823–2825; (*c*) M. R. M. Andreae and A. P. Davis, *Tetrahedron: Asymmetry*, 2005, **16**, 2487–2492; (*d*) F. Calderon, R. Fernandez, F. Sanchez and A. Fernandez-Mayoralas, *Adv. Synth. Catal.*, 2005, **347**, 1395–1403; (*e*) Z. An, W. H. Zhang, H. M. Shi and J. He, *J. Catal.*, 2006, **241**, 319–327; (*f*) D. Font, C. Jimeno and M. A. Pericas, *Org. Lett.*, 2006, **8**, 4653–4655; (*g*) A. Banon-Caballero, G. Guillena and C. Najera, *Green Chem.*, 2010, **12**, 1599–1606; (*h*) E. G. Doyaguez, F. Calderon, F. Sanchez and A. Fernandez-Mayoralas, *J. Org. Chem.*, 2007, **72**, 9353–9356.

4 (*a*) P. X. Zhou, S. Z. Luo and J. P. Cheng, *Org. Biomol. Chem.*, 2011, **9**, 1784–1790; (*b*) D. E. Siyutkin, A. S. Kucherenko and S. G. Zlotin, *Tetrahedron*, 2010, **66**, 513–518; (*c*) J. Shah, H. Blumenthal, Z. Yacob and J. Liebscher, *Adv. Synth. Catal.*, 2008, **350**, 1267–1270; (*d*) P. Kotrusz, I. Kmentova, B. Gotov, S. Toma and E. Solcaniova, *Chem. Commun.*, 2002, 2510–2511; (*e*) T. P. Loh, L. C. Feng, H. Y. Yang and J. Y. Yang, *Tetrahedron Lett.*, 2002, **43**, 8741–8743.

5 (*a*) S. Chandrasekhar, N. R. Reddy, S. S. Sultana, C. Narsihmulu and K. V. Reddy, *Tetrahedron*, 2006, **62**, 338–345; (*b*) S. Chandrasekhar, C. Narsihmulu, N. R. Reddy and S. S. Sultana, *Tetrahedron Lett.*, 2004, **45**, 4581–4582; (*c*) Y. Y. Peng, S. J. Peng, Q. C. Wang and J. P. Cheng, *Chin. J. Chem.*, 2007, **25**, 356–363.

6 (*a*) S. Aratake, T. Itoh, T. Okano, N. Nagae, T. Sumiya, M. Shoji and Y. Hayashi, *Chem.–Eur. J.*, 2007, **13**, 10246–10256; (*b*) X. H. Chen, S. W. Luo, Z. Tang, L. F. Cun, A. Q. Mi, Y. Z. Jiang and L. Z. Gong, *Chem.–Eur. J.*, 2007, **13**, 689–701; (*c*) J. Mlynarski and J. Paradowska, *Chem. Soc. Rev.*, 2008, **37**, 1502–1511.

7 (*a*) K. Kacprzak and J. Gawroński, *Synthesis*, 2001, **7**, 961–998; (*b*) A. B. Zaitsev and H. Adolfsson, *Synthesis*, 2006, **11**, 1726–1756; (*c*) T. Marcelli and H. Hiemstra, *Synthesis*, 2010, **8**, 1229–1279.

8 (*a*) J. R. Chen, X. L. An, X. Y. Zhu, X. F. Wang and W. J. Xia, *J. Org. Chem.*, 2008, **73**, 6006–6009; (*b*) J. Zhou, V. Wakchaure, P. Kraft and B. List, *Angew. Chem., Int. Ed.*, 2008, **47**, 7656–7658; (*c*) B. L. Zheng, Q. Z. Liu, C. S. Guo, X. L. Wang and L. He, *Org. Biomol. Chem.*, 2007, **5**, 2913–2915.

9 R. P. Singh, K. Bartelson, Y. Wang, H. Su, X. J. Lu and L. Deng, *J. Am. Chem. Soc.*, 2008, **130**, 2422–2423.

10 (a) H. M. Li, Y. Q. Wang and L. Deng, *Org. Lett.*, 2006, **8**, 4063–4065; (b) G. Bartoli, M. Bosco, A. Carlone, F. Pesciaioli, L. Sambri and P. Melchiorre, *Org. Lett.*, 2007, **9**, 1403–1405; (c) W. Chen, W. Du, L. Yue, R. Li, Y. Wu, L. S. Ding and Y. C. Chen, *Org. Biomol. Chem.*, 2007, **5**, 816–821.

11 P. Hammar, T. Marcelli, H. Hiemstra and F. Himo, *Adv. Synth. Catal.*, 2007, **349**, 2537–2548.

12 (a) A. L. Tillman, J. Ye and D. J. Dixon, *Chem. Commun.*, 2006, 1191–1193; (b) T. Liu, H. Cui, J. Long, B. Li, Y. Wu, L. Ding and Y. Chen, *J. Am. Chem. Soc.*, 2007, **129**, 1878–1879.

13 (a) P. F. Li, Y. C. Wang, X. M. Liang and J. X. Ye, *Chem. Commun.*, 2008, 3302–3304; (b) X. J. Lu and L. Deng, *Angew. Chem., Int. Ed.*, 2008, **47**, 7710–7713; (c) G. S. Luo, S. L. Zhang, W. H. Duan and W. Wang, *Synthesis*, 2009, **9**, 1564–1572; (d) J. W. Xie, W. Chen, R. Li, M. Zeng, W. Du, L. Yue, Y. C. Chen, Y. Wu, J. Zhu and J. G. Deng, *Angew. Chem., Int. Ed.*, 2007, **46**, 389–392; (e) J. X. Ye, D. J. Dixon and P. S. Hynes, *Chem. Commun.*, 2005, 4481–4483; (f) B. Vakulya, S. Varga, A. Csámpai and T. Soós, *Org. Lett.*, 2005, **7**, 1967–1969; (g) J. P. Malerich, K. Hagihara and V. H. Rawal, *J. Am. Chem. Soc.*, 2008, **130**, 14416–14417; (h) L. T. Dong, R. J. Lu, Q. S. Du, J. M. Zhang, S. P. Liu, Y. N. Xuan and M. Yan, *Tetrahedron*, 2009, **65**, 4124–4129.

14 (a) H. Y. Jiang, C. F. Yang, C. Li, H. Y. Fu, H. Chen, R. X. Li and X. J. Li, *Angew. Chem., Int. Ed.*, 2008, **47**, 9240–9244; (b) W. He, B. L. Zhang, R. Jiang, P. Liu, X. L. Sun and S. Y. Zhang, *Tetrahedron Lett.*, 2006, **47**, 5367–5370.

15 (a) X. W. Wang, C. M. Reisinger and B. List, *J. Am. Chem. Soc.*, 2008, **130**, 6070–6071; (b) X. J. Lu, Y. Liu, B. F. Sun, B. Cindric and L. Deng, *J. Am. Chem. Soc.*, 2008, **130**, 8134–8135.

16 W. Chen, W. Du, Y. Z. Duan, Y. Wu, S. Y. Yang and Y. Z. Chen, *Angew. Chem., Int. Ed.*, 2007, **46**, 7667–7670.

17 H. Brunner and M. A. Baur, *Eur. J. Org. Chem.*, 2003, 2854–2862.

18 (a) S. H. Oh, H. S. Rho, J. W. Lee, J. E. Lee, S. H. Youk, J. Chin and C. E. Song, *Angew. Chem., Int. Ed.*, 2008, **47**, 7872–7875; (b) H. S. Rho, S. H. Oh, J. W. Lee, J. Y. Lee, J. Chin and C. E. Song, *Chem. Commun.*, 2008, 1208–1210.

19 P. Yu, J. He and C. X. Guo, *Chem. Commun.*, 2008, 2355–2357.

20 (a) X. Shi, J. Liu, C. M. Li and Q. H. Yang, *Inorg. Chem.*, 2007, **46**, 7944–7952; (b) Y. Z. Li, T. Kunitake, Y. Aoki and E. Muto, *Adv. Mater.*, 2008, **20**, 2398–2404; (c) S. L. Burkett, N. Ko, N. D. Stern, J. A. Caissie and D. Sengupta, *Chem. Mater.*, 2006, **18**, 5137–5143; (d) X. B. Ma, J. Liu, L. S. Xiao, R. Chen, J. Q. Zhou and X. K. Fu, *J. Mater. Chem.*, 2009, **19**, 1098–1104.

21 (a) A. G. Hu, H. L. Ngo and W. B. Lin, *J. Am. Chem. Soc.*, 2003, **125**, 11490–11491; (b) B. W. Gong, X. K. Fu, J. X. Chen, Y. D. Li, X. C. Zou, X. B. Tu, P. P. Ding and L. P. Ma, *J. Catal.*, 2009, **262**, 9–17; (c) D. Lanari, F. Montanari, F. Marmottini, O. Piermatti, M. Orrù and L. Vaccaro, *J. Catal.*, 2011, **277**, 80–87; (d) T. T. Chen, X. B. Ma, X. J. Wang, Q. Wang, J. Q. Zhou and Q. Tang, *Dalton Trans.*, 2011, **40**, 3325–3335; (e) X. C. Zou, X. K. Fu, Y. D. Li, X. B. Tu, S. D. Fu, Y. F. Luo and X. J. Wu, *Adv. Synth. Catal.*, 2010, **352**, 163–170; (f) X. J. Wu, X. B. Ma, Y. L. Ji, Q. Wang, X. Jia and X. K. Fu, *J. Mol. Catal. A: Chem.*, 2007, **265**, 316–322.

22 (a) X. J. Wang, X. B. Ma, T. T. Chen, X. L. Qin and Q. Tang, *Catal. Commun.*, 2011, **12**, 583–588; (b) X. B. Ma, Y. H. Wang, W. Wang and J. Cao, *Catal. Commun.*, 2010, **11**, 401–407; (c) K. L. Huang, J. H. Yu, G. M. Wang, Y. Li and R. R. Xu, *Eur. J. Inorg. Chem.*, 2004, 2956–2960; (d) Z. Xu, X. B. Ma, Y. Y. Ma, Q. Wang and J. Q. Zhou, *Catal. Commun.*, 2009, **10**, 1261–1266.

23 X. B. Ma and X. K. Fu, *J. Mol. Catal. A: Chem.*, 2004, **208**, 129–133.

24 R. Murugavel, A. Choudhury, M. G. Walawalkar, R. Pothiraja and C. N. R. Rao, *Chem. Rev.*, 2008, **108**, 3549–3655.

25 J. C. Amicangelo and W. R. Leenstra, *Inorg. Chem.*, 2005, **44**, 2067–2073.

26 K. S. W. Sing, D. H. Everett, R. A. W. Haul, L. Moscou, R. A. Pierotti, J. Rouquerol and T. Siemieniewska, *Pure Appl. Chem.*, 1985, **57**, 603–619.

27 (a) C. L. Wu, X. K. Fu and S. Li, *Tetrahedron*, 2011, **67**, 4283–4290; (b) L. S. Zu, H. H. Xie, H. Li, J. Wang and W. Wang, *Org. Lett.*, 2008, **10**, 1211–1214; (c) D. Font, C. Jimeno and M. A. Pericas, *Org. Lett.*, 2006, **8**, 4653–4655; (d) Y. X. Liu, Y. N. Sun, H. H. Tan, W. Liu and J. C. Tao, *Tetrahedron: Asymmetry*, 2007, **18**, 2649–2656; (e) M. Gruttadauria, F. Giacalone, A. M. Marculescu, M. P. Lo, S. Riela and R. Noto, *Eur. J. Org. Chem.*, 2007, 4688–4698.

28 (a) J. G. Hernández and E. Juaristi, *J. Org. Chem.*, 2011, **76**, 1464–1467; (b) C. L. Wu, X. K. Fu, X. B. Ma and S. Li, *Tetrahedron: Asymmetry*, 2010, **21**, 2465–2470.